Acta Montanistica Slovaca
ISSN 1335-1788
actamont.tuke.sk

Dynamic Response Characteristics of Foundation of Mined-out Areas under High-speed Railway Load

Kunpeng SHI[1], Shuren WANG[2], Weibin MA[3], Wenxue CHEN[4] and Marcin RABE[5]*

Authors' affiliations and addresses:
[1] Highway Institute, Henan College of Transportation, Zhengzhou 451460, China
e-mail: 444583054@qq.com

[2] School of Civil Engineering, Henan Polytechnic University, Jiaozuo 454003, China
e-mail: shurenwang@hpu.edu.cn

[3] Railway Engineering Research Institute, China Academy of Railway Sciences Corporation Limited, Beijing 100081, China
e-mail: dwangfei@163.com

[4] Department of Civil & Building Engineering, University of Sherbrooke, Sherbrooke J1K 2R1, Canada
e-mail: Wenxue.chen@usherbrooke.ca

[5] Management Institute, University of Szczecin, Szczecin, 70-453, Poland
e-mail: marcin.rabe@usz.edu.pl

***Correspondence:**
Shuren Wang, School of Civil Engineering, Henan Polytechnic University, Jiaozuo 454003, China
tel.:+86 15738529570
e-mail: shurenwang@hpu.edu.cn

Funding information:
Zhongyuan Science and Technology Innovation Leading Talent Program (244200510005), Key Project of Natural Science Foundation of Henan Province (232300421134), First-Class Discipline Implementation of Safety Science and Engineering of Henan Province (AQ20230103), National Scholarship Fund of China [2023], and Opening Fund of Key Laboratory of High-speed Railway Engineering, Ministry of Education, China [2023].

Acknowledgement:
The authors would like to express their sincere gratitude to the editor and reviewers for their valuable comments, which have greatly improved this paper.

How to cite this article:
Shi, K.P., Wang, S.R. Ma, W.B., Chen, W.X. and Rabe, M. (2024). Dynamic response characteristics of foundation of mined-out areas under high-speed railway load. *Acta Monstanistica Slovaca*, Volume 29 (1), 26-38

DOI:
https://doi.org/10.46544/AMS.v29i1.03

Abstract
To reveal the dynamic response characteristics of the foundation of mined-out areas (MOA) under the high-speed railway (HSR) load is important for predicting settlement and safety assessment of the foundation. Taking MOA of Dianshang under the Taiyuan-Jiaozuo HSR as the engineering background, the model experiments and numerical analysis were employed to reveal the dynamic response of both subgrade and the foundation of the HSR, as well as the attenuation law of the acceleration in the overlying strata of the MOA. Results show that within the full frequency range of the HSR load, the dynamic response of the foundation increases with the increase in load frequency. When the depth exceeds 6 m, the dynamic response of the foundation initially increases and subsequently decreases with the increase in load frequency. Contrasted with single-point loading, the superposition effect and moving effect of the HSR load will form a dynamic response superposition zone within 1-4 m below the subgrade, leading to a significant enhancement of the dynamic response of the foundation. Compared to HSR axle load, the driving speed of HSR has a greater impact on the acceleration of both the subgrade and foundation. The obtained conclusions provide a reference for the safety operation of the HSR crossing the MOA.

Keywords
Taijiao high-speed railway, Mined-out areas, Foundation, Model experiment, Dynamic response.

Introduction

As the construction density of China's high-speed railway (HSR) continues to increase, some HSRs must traverse the mined-out areas (MOA). When HSRs cross the MOA, the dynamic stability of the foundation is not only weakened under the action of the HSR load but also leads to excessive cumulative deformation. In severe cases, this may result in instability and damage to the HSR's railway structure.

The dynamic response of the subgrade and foundation are crucial issues that affect the safety driving of the HSR and reduce large-scale maintenance (Wang and Hu, 2024). Currently, some research on the dynamic characteristics of the foundation under the HSR load is still in its initial exploratory stage. There is also an insufficient understanding of the safety evaluation of damaged foundations in MOA under the HSR load and its dynamic stability (Chen et al., 2023; Liu et al., 2023; Zhang et al., 2024).

The HSR crossing MOA presents a unique geotechnical engineering problem, bringing potential risks and new challenges to the construction and safety driving of the HSR. Therefore, investigating the dynamic response characteristics and dynamic stability of the foundation of the MOA under the HSR vibration load is of significant theoretical significance and practical engineering value for the HSR crossing the MOA.

State of the Art

When HSR crosses the MOA, the foundation of the MOA undergoes the vibration under the action of the HSR load, resulting in dynamic responses such as dynamic stress and vibration acceleration. The vibration acceleration is an important index for assessing the vibration of HSR load on the foundation of the MOA (Ramos et al., 2022; Tian et al., 2020). Some scholars have studied the dynamic response of the HSR embankment. For example, Li et al. (2021) studied the dynamic response of the embankment under the HSR load using the model test. Wang (2023) conducted on-site dynamic testing and evaluated the ballast track subgrade of the HSR. The field tests on high embankments were conducted to investigate the high-strength and deformation characteristics of the train embankment (Yang et al., 2022; Watanabe et al., 2021). Costa et al. (2018) evaluated the stability of the embankment soil under the train loading. Tran et al. (2023) built a new computational model for analyzing the dynamic response of the rail on non-uniform foundations. However, these exploratory studies did not involve the dynamic response and acceleration distribution characteristics of the foundation of the MOA under the HSR cyclic load conditions.

To explore the dynamic properties of the roadbed in the transition section of the road bridge, Qu et al. (2024) conducted a comparative analysis of the spectrum response characteristics and vibration amplitudes of embankments in the transition section. They also evaluated the dynamic stability of the roadbed using field experiments. Tehrani et al. (2024) explored the effect of pile-soil interaction on the dynamic performance of railway bridges through full-scale model experiments. Using numerical simulations, Xu et al. (2024) explored the deformation characteristics and stability of bridge-tunnel structures under single-point vibration loading. Guan et al. (2023) studied the variation of energy attenuation coefficients of the helical pile composite foundation under train loading through model experiments. Yin et al. (2023) analyzed the time-frequency distribution patterns of the acceleration of foundation-track-train structures. Du et al. (2024) explored the stress change path of heavy-duty railway embankments under train loading by establishing a three-dimensional dynamic model. However, these studies did not involve the superposition and moving effects of the HSR loading.

Zhang et al. (2024) discussed the dynamic stability of the railway foundation in the Kanerjing area through model experiments. Wang et al. (2021) analyzed the coordination deformation adaptability between the high-speed railway track structures and subgrade, subgrade, and foundation of the MOA and discussed the evolutionary trends of structures and accumulated deformation characteristics of the overlying strata of the MOA under the HSR load. Yan (2022) researched exploration techniques of MOA, design principles, grouting construction processes, quality inspection, and acceptance for the Nanning-Qinzhou high-speed railway crossing MOA. Currently, there is considerable research on the remaining deformation and grouting reinforcement of the foundation of the MOA, but the dynamic analysis of the foundation under the HSR load is not yet deep enough.

This study established a finite element dynamic model of train-embankment-ground in MOA, and the indoor dynamic similarity model experiments were conducted to validate the numerical dynamic model. By using the established dynamic calculation model, the attenuation and distribution laws of vibration acceleration of the foundation of the MOA under different speeds and axle loads were studied. The effects of the moving effect and superposition effect of the HSR loads on the foundation were analyzed. The results of this study can provide a theoretical basis for the safety operation of HSR crossing the MOA.

The rest of this study is organized as follows. The material and methods section describes the relevant background and research methods. Then, the results and discussion are given, and finally, the conclusions are summarized.

Materials and methods

Model experiment

The Taiyuan-Jiaozuo HSR traversed the MOA of Dianshang in Shanxi Province, China. The indoor experiments were conducted using a model test platform by taking the Taiyuan-Jiaozuo HSR crossing the MOA as the background. The size of this platform was 250 cm × 50 cm × 210 cm.

Similarity relationship and determination of similar materials. Considering the dimension of the test platform and the performance parameters of the loading device, the similarity ratio for the dynamic loading model of the foundation of the MOA was determined to be 0.01. The average density of the rock layer was 2000 kg/m^3, while the density of a similar material was 1680 kg/m^3. The density similarity constant could be obtained C_ρ=1680/2000=0.84, which was used to determine the similarity ratios of physical quantities in this experimental model. The materials parameters of the model are displayed in Tab. 1.

According to the similarity ratios of the model, the natural fine river sand with a particle size of less than 5 mm was selected as the aggregate. The travertine and plaster were employed as the binding materials. Considering that gypsum as a binding material had a short setting time, it was inconvenient for the experimental operation process and affected the physical and mechanical properties of similar materials. Therefore, a retarder was added to similar materials, and the borax was selected as the retarder and configured into a 1% concentration borax solution. In addition, the larger particles of mica powder or mica sheets were used to simulate the stratification of rock layers (Shi et al., 2023).

Tab. 1. Materials parameters of the model.

Name	Density [kg/m^3]	Cohesion strength [kPa]	Internal friction angle [°]	Elastic modulus [MPa]	Poisson' ratio
Subgrade	1860	25	22	160	0.20
Fill	1870	30	21	1.19	0.28
Loess	1920	31	26	4.01	0.23
Mudstone	2200	1560	25	5500	0.19
Sandy mudstone	2100	2730	26	5700	0.23
Medium sandstone	1960	2500	22	4500	0.20
Siltstone	2300	1600	28	7500	0.20
Coal	1400	530	23	1000	0.30
Fine stone	1970	3500	32	9860	0.20
Rail	7800	/	/	206000	0.23
Sleeper	2400	/	/	35500	0.10
Plate	2400	/	/	30000	0.10

Experimental equipment and layout of measurement points. The size of the experimental model was 200 cm × 30 cm × 93 cm, with a thickness of 4.05 cm for the coal seam. After laying and compacting the experimental materials and allowing them to solidify, monitoring equipment, such as soil pressure cells and accelerometers, was installed. Then, the coal was excavated to construct the MOA. The experimental model is displayed in Fig. 1.

To acquire the dynamic response of the foundation of the MOA under the HSR load and the internal stress distribution status of the model while considering the cost-effectiveness of the experiment, the highly sensitive dynamic soil pressure boxes and acceleration sensors were embedded inside a similar model. These devices were used to monitor the dynamic response inside the model. The arrangement of the dynamic soil pressure boxes and acceleration sensors is shown in Fig. 2.

In this experiment, the DH1301 frequency signal generator was utilized to conduct a frequency sweep of the HSR load over the entire frequency range for the MOA. Simultaneously, an actuator was controlled to apply a single-point loading of the HSR to the top of the model. A microcomputer system controlled the vibration signal applied in the experiment and transmitted the actuator through the signal generator and power amplifier. The actuator applied the vibration load to the top of the subgrade, and the dynamic response was monitored by the sensors embedded in the subgrade and the foundation of the MOA. The signal acquisition instrument converts the dynamic responses captured by the dynamic soil pressure boxes and acceleration sensors into digital signals and transmits them to the computer. All data obtained from the experiment were processed within the testing system, as displayed in Fig. 3.

Fig.1. Indoor physical similarity model.

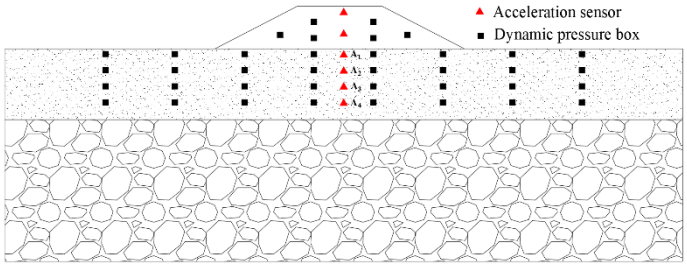

Fig.2. Layout of the test sensor.

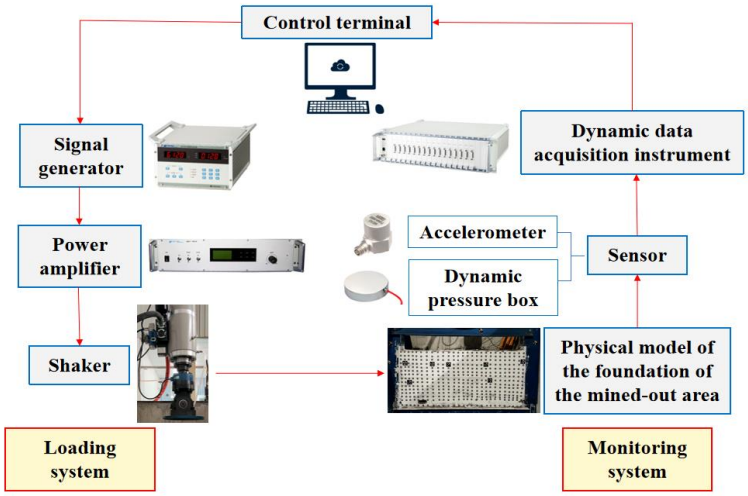

Fig. 3. Experimental testing system.

Numerical simulation analysis

The computational model. A numerical model was established by using Abaqus software, and the dimension of the numerical model was 200 m × 90 m × 110 m. The 3D computational model of the foundation-embankment-track in the MOA was illustrated in Fig. 4. Since the railway system and soil layers were both in a small strain state under the high-speed railway vibration load, the linear elastic models were employed for both the railway system and soil layers. In addition, the infinite element boundary conditions were selected to absorb body waves at the boundaries of the computational model, reducing the impact of the boundaries on the computational results.

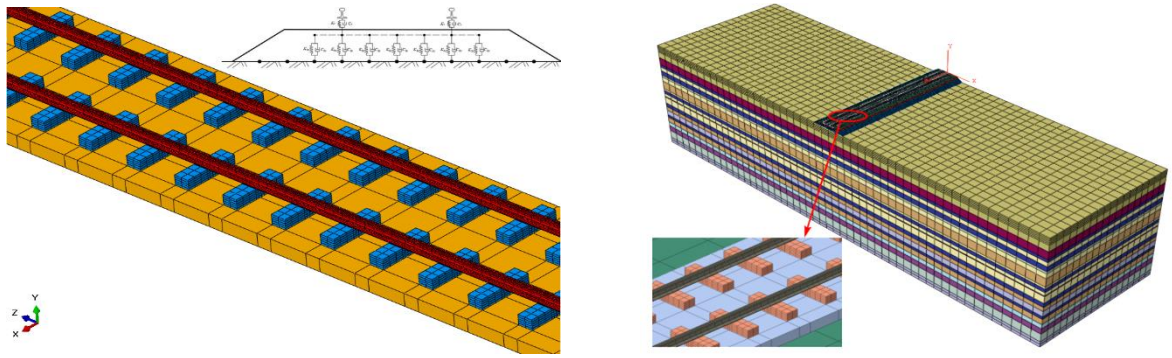

(a) Railway system *(b) Numerical model*

Fig. 4. Three-dimensional numerical analysis model of foundation-embankment-track.

Model dynamic loading. During the quasi-static calibration period, all the test components were repeatedly adjusted to confirm proper installation and set before commencing formal testing. The data acquisition instrument was triggered manually on-site to record data automatically. The typical time-history curve of dynamic stress

obtained from monitoring is shown in Fig. 5(a). After preprocessing the acquired monitoring data, including physical unit calibration and noise signal removal, the effective vibration information and clear signal waveform were obtained, as illustrated in Fig. 5(b). The time-history curve of the wheel-rail stress is smooth after preprocessing, with distinct peaks and troughs. The loading and unloading processes of train formations and individual train wheelsets are clearly distinguishable, allowing for accurately determining the periodic characteristics of vibration response. These data can be used to generate time-history curves for the train load in indoor model experiments and numerical simulations.

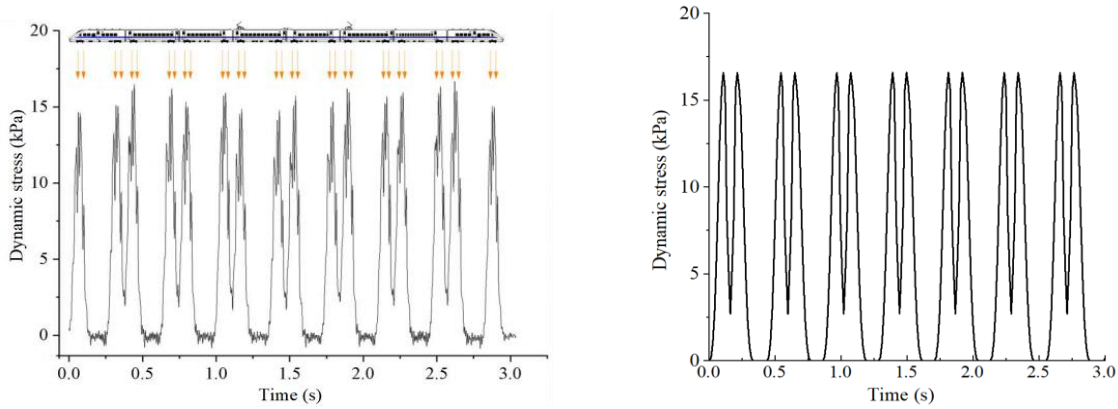

(a) Field test *(b) Model loading*

Fig. 5. Time history curve of wheel-rail stress for a train.

Dynamic response of foundation of MOA under single-point loading

Acceleration response characteristics of foundation in the time domain

The selection of damaged parameters for the foundation significantly impacts the precision of the results obtained from the model of the foundation-embankment-track system. To verify the reliability of the numerical computational analysis and indoor model experiments, this study established the analysis models for the foundation and conducted dynamic response analysis under single-point loading through numerical simulation and indoor experiments. Fig. 6 illustrates a comparison between the acceleration time-history curves derived from simulation analysis and the monitoring results of the model tests.

As shown in Fig. 6, the time-history curves of acceleration on the surface layer of the subgrade and the foundation of the MOA were obtained from both numerical analysis and model experiments under the M-shaped loading, exhibiting similar waveform characteristics. Due to constraints in the experimental laboratory conditions and external interferences, the peak acceleration obtained from the model experiments was slightly smaller than the numerical analysis results. However, the calculation findings are generally aligned with the test findings. Additionally, there is a certain degree of attenuation in peak acceleration along the depth from the subgrade to the foundation, with numerical analysis and model test results showing approximately 50.68% and 53.03% attenuation, respectively, with an error of less than 3%.

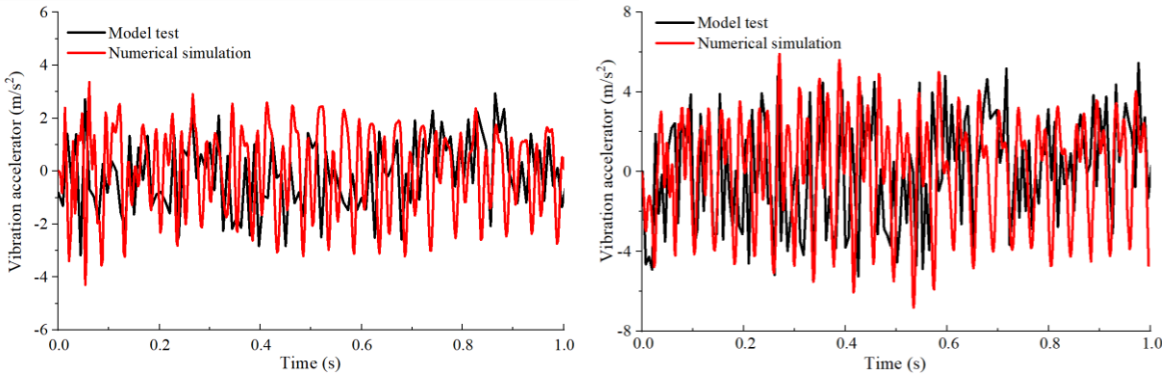

(a) Surface layer of subgrade *(b) Foundation of the MOA*

Fig. 6. Time-history curves of acceleration of typical measurement points for the subgrade and foundation of the MOA.

Fig. 7 shows the distribution properties of the peak vibration acceleration along depth under single-point loading obtained from numerical simulation and indoor model experiments. It is evident that the distribution characteristics of the acceleration along depth are resembled for both numerical simulation and model experiments. The peak vibration acceleration decreases with the increasing depth, and the vibration intensity rapidly attenuates within the subgrade range, demonstrating that the subgrade has a notable attenuating effect on the vertical vibration caused by HSR load. As the foundation depth progressively deepens, the rate of acceleration attenuation slows down and tends to converge, with the influencing depth reaching approximately 10 m below the foundation.

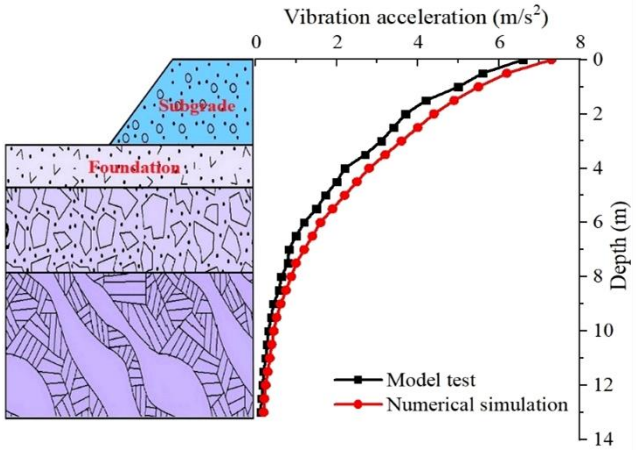

Fig. 7. Acceleration response distributions along depth under single point loading.

To further investigate the attenuation characteristics of the acceleration with depth, the ratio of the vibration acceleration at any depth below the subgrade surface to the vibration acceleration is defined as the acceleration attenuation coefficient ξ_a. Thus, ξ_a can be expressed as:

$$\xi_a = \frac{A_0 - A_i}{A_0} \xi_a = \frac{A_0 - A_i}{A_0} \tag{1}$$

where, A_i represents the peak vibration acceleration at depth i below the subgrade surface, m/s^2. A_0 represents the peak vibration acceleration at the embankment surface, m/s^2.

Fig. 8 shows the vibration acceleration attenuation coefficient along the depth curve. As seen from Fig. 8, the results of numerical analysis and model test present similar trends and distribution characteristics of the vibration acceleration attenuation coefficient ξ_a along the depth, ξ_a decreases with increasing depth. Specifically, as the vibration load of the HSR propagates from the subgrade to the ground surface, the acceleration attenuates by approximately 60%, reaching 90% attenuation at 10 m below the subgrade. Additionally, within the interface between the subgrade and the ground surface and within the foundation range, the vibration acceleration attenuation coefficient ξ_a increases slightly in the model test. This is attributed to the insufficient smoothness of the bottom surface during the preparation of the subgrade, resulting in inadequate contact with the foundation surface.

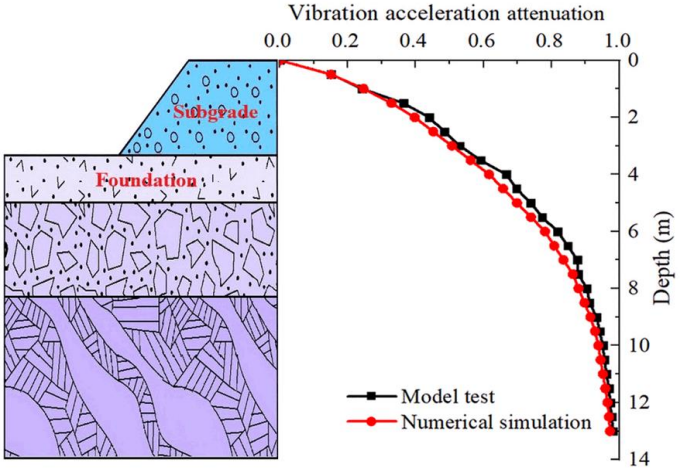

Fig. 8. Vibration acceleration attenuation coefficient-depth curve.

The definition of the frequency response

The acceleration monitoring data of the foundation of the MOA under linear sine sweep excitation of a high-speed railway was processed using the frequency response function (FRF). The purpose is to eliminate the effect of the load amplitudes caused by HSR operations on the foundation, and the vibration acceleration time domain results can be converted into dynamic responses in the frequency domain (Yang et al., 2022). The expression for the frequency response function is as follows:

$$FRF(\omega) = \frac{S_{\mathrm{FA}}(\omega)}{S_{\mathrm{FF}}(\omega)} FRF(\omega) = \frac{S_{\mathrm{FA}}(\omega)}{S_{\mathrm{FF}}(\omega)} \tag{2}$$

where, $S_{\mathrm{FA}}(\omega)$ represents the cross-power spectral density function between the HSR vibration load and acceleration, and $S_{\mathrm{FF}}(\omega)$ represents the power spectral density function of the HSR vibration load. Their functional expressions are as follows:

$$S_{\mathrm{FA}}(\omega) = \frac{1}{N_S^2}\left[\sum_{n=0}^{N_S-1} F(t)_n e^{-\frac{2\pi imn}{N_S}}\right]\left[\sum_{n=0}^{N_S-1} A(t)_n e^{-\frac{2\pi imn}{N_S}}\right] \tag{3}$$

$$S_{\mathrm{FF}}(\omega) = \frac{1}{N_S^2}\left[\sum_{n=0}^{N_S-1} F(t)_n e^{-\frac{2\pi imn}{N_S}}\right]^2 \tag{4}$$

where, $F(\omega)_{\mathrm{n}}$ represents the HSR vibration load, $A(\omega)_{\mathrm{n}}$ represents the monitored vibration acceleration at the point within the foundation of the MOA, and N_{S} denotes the number of monitoring points, where n = 1, 2, 3, ..., N_{S}, and m = 1, 2, 3, ..., N_{S}.

$$FRF(\omega) = \frac{S_{FA}(\omega)}{S_{FF}(\omega)} = \frac{\frac{1}{N_S^2}\left[\sum_{n=0}^{N_S-1} F(t)_n e^{-\frac{2\pi imn}{N_S}}\right]\left[\sum_{n=0}^{N_S-1} A(t)_n e^{-\frac{2\pi imn}{N_S}}\right]}{\frac{1}{N_S^2}\left[\sum_{n=0}^{N_S-1} F(t)_n e^{-\frac{2\pi imn}{N_S}}\right]^2} = \frac{\sum_{n=0}^{N_S-1} A(t)_n e^{-\frac{2\pi imn}{N_S}}}{\sum_{n=0}^{N_S-1} F(t)_n e^{-\frac{2\pi imn}{N_S}}} \tag{5}$$

Acceleration response characteristics of foundation in the frequency domain

The aforementioned data processing method was utilized to convert the vibration acceleration monitoring results in the foundation from the time domain signals to frequency domain signals. The variation patterns of vibration acceleration frequency response at typical monitoring points in the foundation under different train axle loads can be obtained through denoising and smoothing of the obtained frequency domain signals, as displayed in Fig. 9.

As seen in Fig. 9, there are distinct differences in the dynamic response at different depths within the foundation of the MOA. The closer to the vibration source, the greater the acceleration frequency response. Taking the 20 t train axle load as an example, the vibration acceleration frequency response at monitoring point A_1 in the MOA is greater than that at A_2, with an average difference of 8.62 dB. A_2 is greater than A_3, with an average difference of 9.04 dB. At the same time, A_3 is greater than A_4, with an average difference of 10.86 dB. Overall, the vibration acceleration frequency response at monitoring points A_2, A_3, and A_4 in the foundation is attenuated by 10.78%, 11.30%, and 13.58%, respectively, compared to monitoring point A_1.

The vibration acceleration frequency responses at monitoring points A_1, A_2, and A_3 in the foundation, which are closer to the vibration source, increase with increasing frequency, while the vibration acceleration frequency response at monitoring point A_4, which is farther from the vibration source, initially increases and subsequently decreases with increasing frequency. The frequency corresponding to this decrease point increases with the axle load increases. This indicates that the effect of high-frequency components on the acceleration level of the deeper part of the foundation gradually strengthens as the train axle weight increases.

As the frequency of the HSR load rises, the fluctuation of the acceleration level curve of the foundation becomes more pronounced. This is mainly due to the increase in vibration load frequency, which not only increases the acceleration level of the foundation but also exacerbates the surrounding environmental vibrations, thereby increasing the interference with the experimental model itself. Further analysis reveals that the fluctuation of the dynamic response in the MOA gradually weakens with the axle load increases. Thus, it can be inferred that the sensitivity of vibration acceleration frequency response in the foundation to the load frequency surpasses train axle weight.

The overall acceleration level of the foundation closer to the vibration source exhibits a positive correlation with the loading frequency, and its variation characteristics are closely related to the magnitude and range of the

loading frequency. The fluctuation of the acceleration level curve of the foundation is more pronounced in the low-frequency band than in the high-frequency band. Additionally, as the distance increases, the vibration acceleration response gradually weakens. This is mainly caused by the presence of damping in the model materials, leading to continuous attenuation of stress waves during the propagation process.

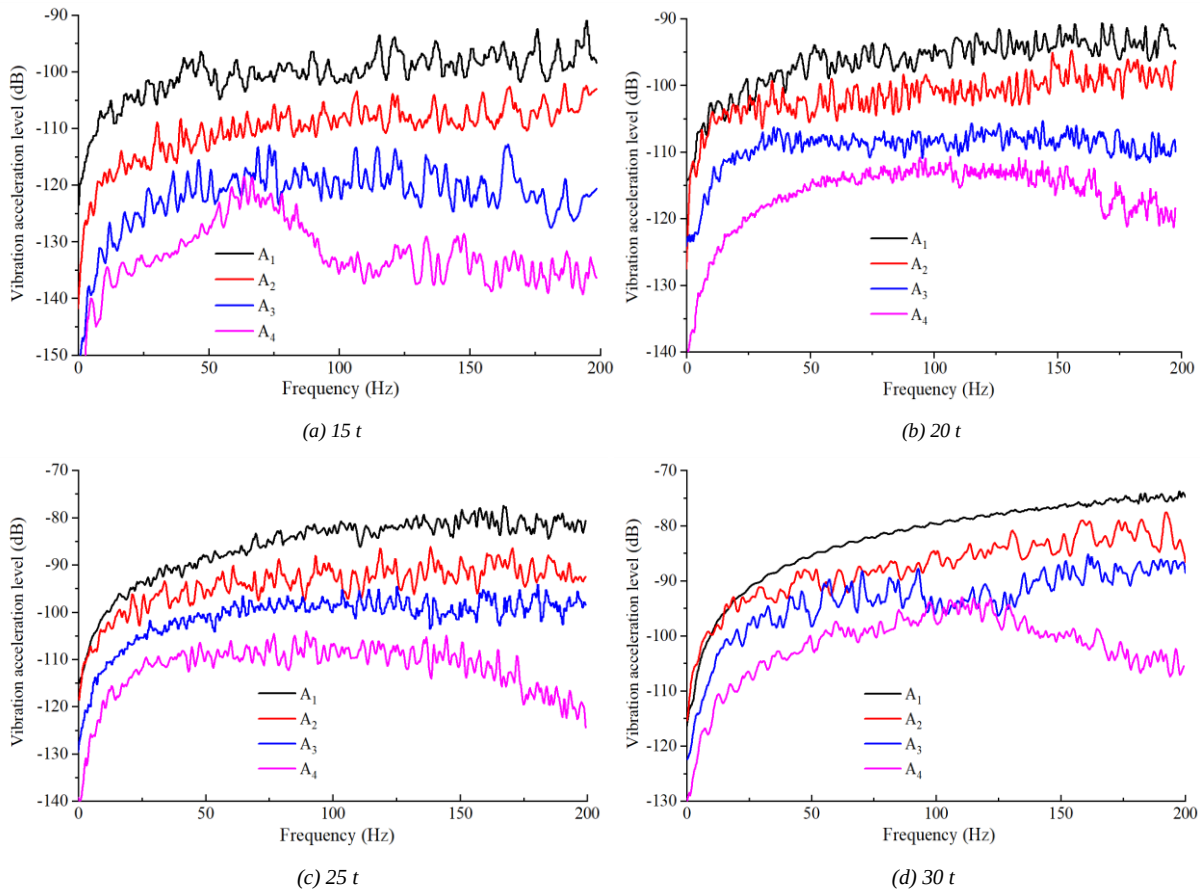

Fig. 9. Comparison of frequency response curves of typical measuring points of the foundation under different train axle loads.

Dynamic response of foundation under train moving load

The reliability of model experiments and numerical simulations under single-point load has been verified in the preceding sections. However, the load generated by high-speed trains is not a single-point vibration but varies continuously in space and time. Therefore, the user-defined load subroutine (Subroutine dload) provided by Abaqus was used to simulate the moving load generated by train movement. The different load moving speeds and sizes can be simulated for analysis by adjusting the parameters of the user-defined load subroutine.

Acceleration response analysis of Foundation. Fig. 10 shows the peak vibration accelerations of the high-speed railway track system under single-point load and moving load. The peak acceleration under the HSR load exceeds the single-point vibration load. Under the HSR load, the vibration acceleration of the rail increases by approximately 91.22%, at the sleeper by 87.02%, at the surface of the subgrade by 96.73%, and at the surface of the foundation by 103.65%. This indicates that considering the moving effect of the HSR load will enhance the vibration strength of both the subgrade and the foundation. This change is also related to the superposition effect of the multiple excitation points at a certain monitoring point. Therefore, it is essential to explore both the moving effect and the superposition effect of HSR load when studying the dynamic response of the foundation.

The distribution characteristics of the acceleration of the foundation at different moments as the high-speed train travels from right to left at a velocity of 250 km/h are displayed in Fig. 11. The acceleration of the foundation moves with the movement of the HSR load. The peak vibration acceleration of the model is primarily focused in the subgrade and shallow foundation directly below the wheel-rail contact area, and it propagates towards the surroundings and the lower part of the roadbed. Additionally, the acceleration induced by HSR is mostly attenuated in the surface layers of the subgrade and foundation, with minimal impact on the deeper foundation below 10 m. Furthermore, due to the rapid attenuation of the foundation's acceleration, the vibration acceleration's superposition effect between adjacent wheel-rail pairs in the direction of train travel is not significant.

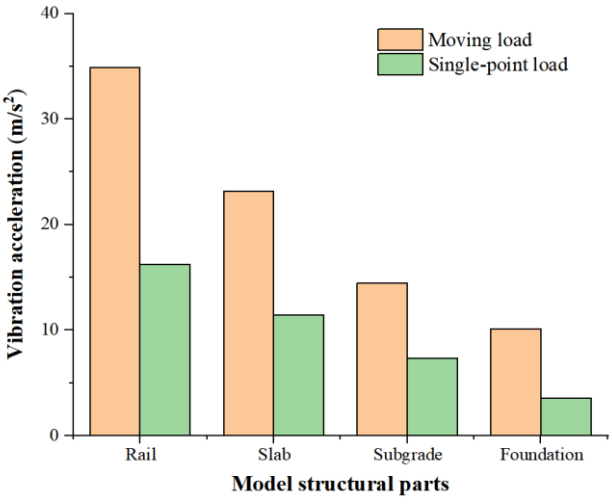

Fig. 10. Vibration acceleration of the model structure parts under single-point load and moving load

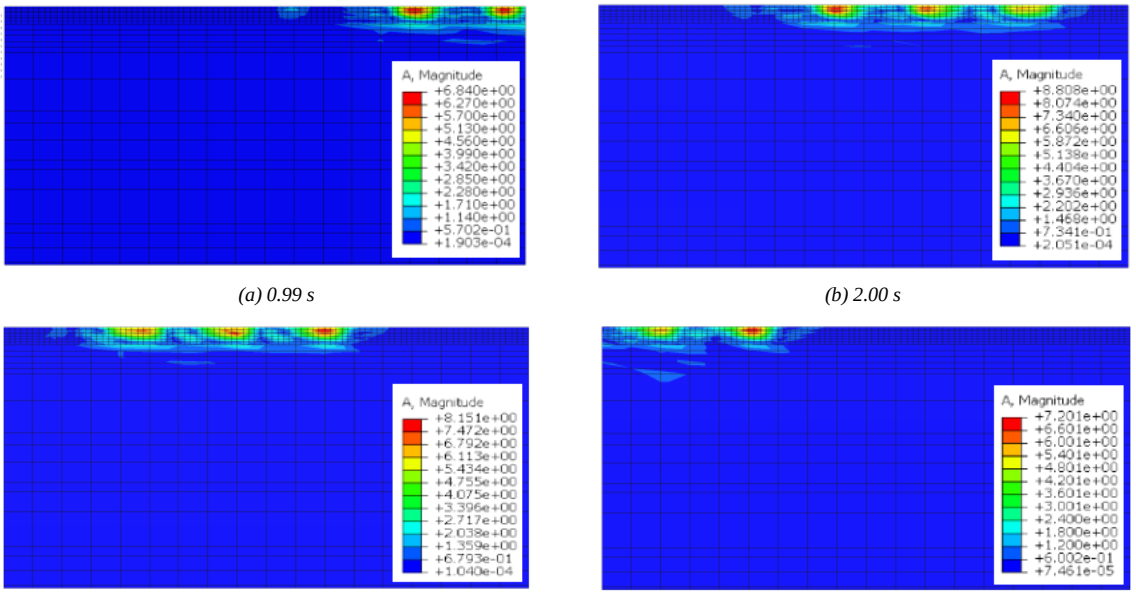

(a) 0.99 s *(b) 2.00 s*

(c) 2.56 s *(d) 3.5 s*

Fig. 11. Distribution characteristics of the vibration acceleration of the foundation at different moments.

Statistical analysis of acceleration of foundation. To study the acceleration distribution laws of the foundation under the action of the HSR moving loads, the longitudinal distribution of the acceleration in the foundation under different HSR driving conditions is displayed in Fig. 12. The vibration acceleration of the foundation sharply attenuates along the centerline of the subgrade to both sides under the different high-speed train operating conditions, and the attenuation curve presents symmetric distribution about the centerline of the subgrade. Specifically, the acceleration of the surface layer of the foundation is located directly under the wheel-rail load and sharply attenuates within a 10 m range along the longitudinal direction. Taking two operating conditions as examples, namely, a train axle load of 30 t (250 km/h) and a velocity of 350 km/h (20 t), the acceleration of the foundation decreased from 11.54 m/s² and 13.57 m/s² to 3.93 m/s² and 4.61 m/s², respectively, representing a reduction of approximately 66%. As the vibration acceleration propagates to the distance, its attenuation rate gradually slows down. When the vibration acceleration is transmitted 20 m away, it attenuates to 0.76 m/s² and 0.93 m/s². Compared with 10 m, representing only about a 20% reduction. Additionally, under different conditions, such as train axle load and HSR velocity, the transmission law of the acceleration along the longitudinal direction is similar. It presents a pattern where the attenuation rate initially decreases rapidly with increasing distance, and within a 20 m range, the vibration acceleration decreases by over 90%. Beyond 20 m, the attenuation rate gradually slows down with increasing distance, eventually stabilizing.

Fig. 13 shows the depth distribution laws of the acceleration along depth under different high-speed train operating conditions. Under the influence of HSR moving loads, the attenuation pattern of the acceleration along depth differs from that under single-point loading. Specifically, owing to the superposition effect of the HSR

moving loads in the subgrade, the acceleration decreases initially and then increases with increasing depth, reaching a peak at about 2.5 m. When surpassing the influence range of the superposition effect of the train moving loads, the vibration acceleration rapidly decreases with increasing depth, and the vibration intensity also attenuates quickly within the subgrade range. Taking two operating conditions as examples, namely, a train axle load of 30 t (250 km/h) and a velocity of 350 km/h (20 t), the acceleration at the surface of the foundation is 11.32 m/s² and 12.28 m/s², respectively. Compared with the vibration acceleration of the surface of the subgrade, the vibration acceleration at the surface layer of the foundation decreases by approximately 23.52% and 25.17%, respectively. Compared with the single-point loading case, the acceleration at the goaf foundation increases by approximately 3 times under the influence of the HSR moving loads. Consequently, it can be concluded that the superposition effect of the HSR moving loads leads to a greater vibration intensity in the foundation, thereby posing greater potential risks to its stability.

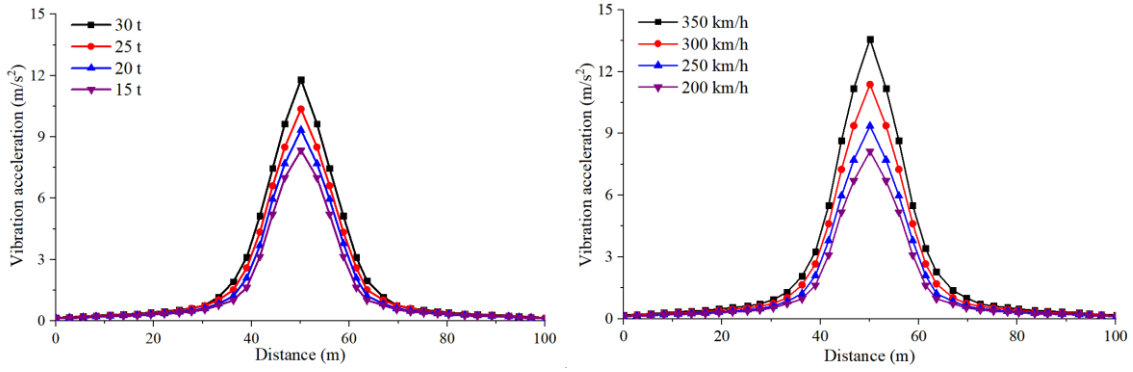

(a) Different train axle loads (250 km/h) *(b) Different driving speeds (20 t)*

Fig. 12. Distribution law of vibration acceleration along direction under different train operating conditions.

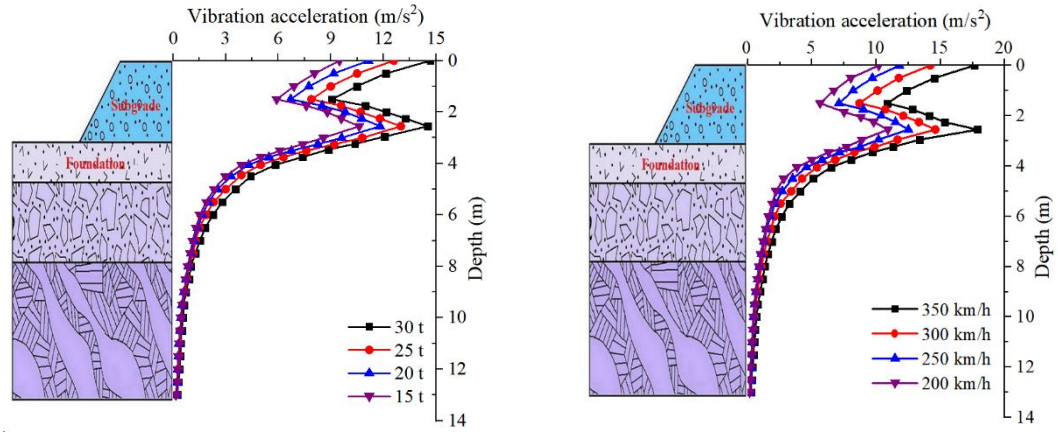

(a) Different train axle loads (250 km/h) *(b) Different driving speeds (20 t)*

Fig. 13. Distribution law of vibration acceleration along depth under different train operating conditions.

Influencing factors analysis of the dynamic response of the foundation

To further investigate the relationship between vibration acceleration at typical monitoring points in the foundation and factors such as velocity and train axle load, the high-speed train operational characteristics with train axle loads ranging from 15-30 t and velocities from 200-350 km/h were picked for computational analysis. Fig. 14 illustrates the impact of different operating conditions on the dynamic response of the foundation.

As seen from Fig. 14, it is evident that the vibration acceleration of the foundation increases with the rise in the velocity and train axle load. Specifically, under the condition of operating at 250 km/h, with the increase of the train axle weight ranging from 15-30 t, the vibration acceleration at both the subgrade and foundation surface layers increases by 5.14 m/s² and 4.52 m/s², respectively. Under a 20 t train axle load, as the velocity increases, ranging from 200-350 km/h, the acceleration at both the subgrade and foundation surface layers increases by 5.05 m/s² and 6.72 m/s², respectively. From an overall perspective, when the train velocity is relatively low, the effect of the axle load on the acceleration is relatively small.

Furthermore, the sensitivity of the acceleration of the foundation to the HSR load frequency is much greater than that of the train axle load. The effects of change in HSR operating velocity on the vibration acceleration of

the foundation are mainly due to the rise in HSR velocity exacerbating the unevenness of the track and increasing the frequency of dynamic load application to some extent. Additionally, when the train velocity is low, the rate of increase in vibration acceleration response with HSR velocity is low and changes gently. As the HSR operating velocity gradually increases, the growth rate of the vibration acceleration accelerates, and the dynamic amplification effect of the roadbed becomes more pronounced, further exacerbating the roadbed's dynamic response, reflecting the HSR loads' moving effect.

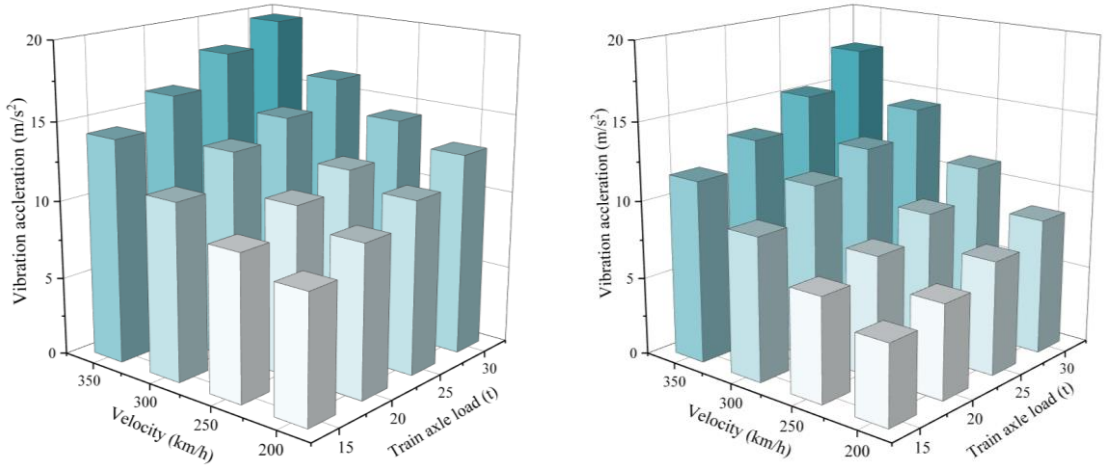

(a) Surface layer of subgrade *(b) Foundation of MOA*

Fig. 14. Effects of different traveling conditions on the dynamic response of vibration acceleration.

Therefore, it is evident that the train velocity seriously impacts the dynamic response of the foundation of the MOA. With the increase in HSR operating velocity, both the safety of HSR operation and the dynamic stability of the foundation deteriorate significantly. When high-speed trains pass through goaf sites, more attention should be given to the impact of the HSR velocity on the dynamic properties of the foundation.

Conclusions

By combining model experiments with numerical simulations, the time-frequency domain dynamic properties of the foundation of the MOA under the single-point loading and HSR moving loads were studied, revealing the attenuation characteristics of the acceleration during propagation. The main conclusions were obtained as follows:

(1) The moving effect of the HSR load will increase the foundation's dynamic response, resulting in the acceleration of the subgrade by approximately 105% and at the foundation surface increased by 41.9%. Meanwhile, the superposition effect of the HSR moving loads resulted in a zone of overlapped dynamic response within 1-4 m below the trackbed, where the vibration acceleration increased by about 2-3 times compared to single-point load. Therefore, when studying the dynamic properties of the foundation, the superposition effect and moving effect of the HSR moving load should be considered.

(2) The frequency response of the foundation is closely associated with the loading frequency and burial depth. The vibration acceleration level near the vibration source increases with increasing frequency, but when the burial depth from the vibration source exceeds 6 m, the acceleration level initially increases and subsequently decreases with the rise of frequency. Furthermore, as the train axle load increases, the frequency of the acceleration level drop point increases, indicating that stress waves strongly impact the acceleration level of the deep part of the foundation in the high-frequency range. However, its fluctuation gradually decreases. Thus, the sensitivity of vibration acceleration frequency response in the foundation to the load frequency surpasses the train axle load.

(3) Compared to train axle load, the HSR operating velocity has a more significant effect on the acceleration response of the roadbed and the foundation. Especially during high-speed train operation, greater attention should be given to the dynamic properties of speeds exceeding 250 km/h and their effects on the stability of the subgrade and the foundation.

This study only studied the dynamic response of the foundation of the MOA. However, due to the stricter requirements of high-speed railways for roadbed settlement, the subsequent research work will investigate the correlation effect between dynamic stress and cumulative deformation of the foundation of the MOA.

Reference

Chen, X., Xiong, Z.M., Chen, Z. (2023). Shaking table test and numerical simulation on subway station in ground fissure area. Engineering Mechanics, 40(7), pp. 228-238. DOI: 10.6052/j.issn.1000-4750.2022.03. 0260.

Costa, P. A., Lopes, P., Cardoso, A. S. (2018). Soil shakedown analysis of slab railway tracks: numerical approach and parametric study. Transportation Geotechnics, 16, pp. 85-96. DOI: 10.1016/j.trgeo.2018.07. 004.

Du, Y. F., Cui, X. Z., Bao, Z. H., Li, X. Y., Hao, J. W., Zhang, S. Q. (2024). Three-dimensional dynamic response analysis of unsaturated subgrade in heavy-haul railways. Journal of the China Railway Society, 2024, pp. 1-9. DOI: 11.2104.U.20240229.1327.002.

Guan, W., Wu, H. G., Pai, L. F., Ma, Z. G., Feng, K. (2023). Acceleration response of part-screw pile composite foundation under long-term train load excitation. Journal of vibration and control, 2023, pp. 2023. DOI: 10.1177/10775463231207138.

Li, X., Bai, M. Z., Wei, Z. J., Li, P. X., Shi, H., Zhang, Y. (2021). Dynamic response and stability analysis of high-speed railway subgrade in karst areas. IEEE Access, 9, pp. 129188-129206. DOI: 10.1109/ACCESS. 2021.3113706.

Liu, Z. Y., Zhao, Y. M., Li, T. F., Wang, L. Y., Zhang, X. G., Zhang, Q. (2023). Study on dynamic response and long-term dynamic stability of high-speed railway subgrade under higher speed conditions. Journal of the China Railway Society, 45(4), pp. 127-138. DOI: 10.3969/j.issn.1001-8360.2023.04.015.

Qu, C. Z., Tan, X. Y., Xiao, Y. J., Wang, Z., Wei, L. (2024). M. Subgrade vibrations and long-term stability of an embankment-bridge transition zone in non-ballasted high-speed railway. Transportation geotechnics, 45, pp. 101199. DOI: 10.1016/j.trgeo.2024.101199.

Ramos, A., Correia, A. G., Calcada, R., Costa, P. A. (2022). Stress and permanent deformation amplification factors in subgrade induced by dynamic mechanisms in track structures. International Journal of Rail Transportation, 10(3), pp, 298-330. DOI: 10.1080/23248378.2021.1922317.

Shi, K. P., Wang, S. R., Chen, Y. B., Yang, W. F., Li, C. L. (2023). Cumulative deformation analysis of foundation of mined-out areas under dynamic loading-a case study of Taijiao high-speed railway. Tehnicki Vjesnik-Technical Gazette, 30(2), pp. 622-630. DOI: 10.17559/TV-20220802045029.

Tehrani, S. A. H., Andersson, A., Zanganeh, A., Battini, J. M. (2024). Dynamic soil-structure interaction of a three-span railway bridge subject to high-speed train passage. Engineering structures, 308, 117296. DOI: 10.1016/j.engstruct.2023.117296.

Tian, T., Li, G. Q., Qi, F. L. (2020). Analysis on acceleration response of tunnel lining under vibration load of train with speed of 300 km/h. Journal of the China Railway Society, 42(6), pp. 112-120. DOI: 10.3969/j.issn.1001-8360.2020.06.015.

Tran, L. H., Hoang, T., Foret, G., Duhamel, D. (2023). Calculation of the dynamic responses of a railway track on a non-uniform foundation. Journal of vibration and control, 29(15), pp. 3544-3553. DOI: 10.1177/10775463221099353.

Wang, R., Hu, Z. P. (2024). Current situation and prospects of 2.5D finite element method for the analysis of dynamic response of railway subgrade. Rock and Soil Mechanics, 45(1), pp. 284-301. DOI: 10.16285/j.rsm.2022.1822.

Wang, S. R., Shi, K. P., Zou, Y. F., Zou, Z. S. (2021). Coupling deformation between non-uniform settlement of track-structure and subgrade of high-speed railway above the mind-out areas. Acta Montanistica Slovaca, 26(4), pp. 620-633. DOI: 10.46544/AMS.v26i4.03.

Wang, S. R., Shi, K. P., Zou, Y. F., Zou, Z. S., Wang, X. C., Li, C. L. (2021). Size effect analysis of scale test model for high-speed railway foundation under dynamic loading condition. Tehnicki Vjesnik- Technical Gazette, 28(5), pp. 1615-1625. DOI: 10.17559/TV-20210208101312.

Wang, Y. (2023). Dynamic stability evaluation of high-speed railway ballasted track subgrade bed structure based on field tests. Railway Construction Technology, (12), pp. 154-256. DOI: 10.3969/j.issn.1009-4539.2023.12.037.

Watanabe, K., Nakajima, S., Fujiwara, T., Yoshii, K., Rao, G. V. (2021). Construction and field measurement of high-speed railway test embankment built on Indian expansive soil"Black Cotton Soil". Soils and Foundations, 61(1), pp. 218-238. DOI: 10.1016/j.sandf.2020.08.008.

Xu, S., Xu, Q., Zhu, Y. Q., Guan, Z. Z., Wang, Z. H., Fan, H. B. (2024). Dynamic response of bridge-tunnel overlapping structures under high-speed railway and subway train loads. Sustainability, 16(2), pp. 848. DOI: 10.3390/su16020848.

Yan, D. (2022). Stability analysis and treatment measures of high-speed railway adjacent to deep coal mine goaf. Journal of Railway Engineering Society, 39(6), pp. 37-42. DOI: 10.3969/j.issn.1006-2106.2022.06.007.

Yang, Q., Zhang, L., Wei, L. M., Nie, Z. H., Nie, R. S., Xu, F., Leng, W. M. (2022). Probability distribution law and design value of dynamic stress amplitude on subgrade surface under high-speed railway trainload. China Civil Engineering Journal, 55(9), pp. 78-93. DOI: 10.15951/j.tmgcxb.21090891.

Yang, W., Yang, L. L., Liang, Y., Qian, Z. H., Guo, W. Q., He, C., Zhou, Y. (2022). Study on the dynamic response characteristics of road-metro tunnels and surrounding soil under train vibration loads. Chinese Journal of Rock Mechanics and Engineering, 41(8), pp. 1659-1670. DOI: 10.13722/j.cnki.jrme.2021.0904.

Yin, Z. H., Zeng, Y., Wei, H. L., Yin, Z., Gao, J. J. (2023). Time-frequency characteristics of vibration acceleration of high-speed railway subgrade under ejection impact load. Journal of Southwest Jiaotong University, 58(1), pp. 219-226. DOI: 10.3969/j.issn.0258-2724.20211034.

Zhang, C., Tian, K. Y., Yuan, S. Y., Zhai, W., Min, Q., Song, J. Y., Chen, W. Z., Liu, X. F. (2024). Stability of shallow-buried Qanat foundation under cyclic load. Journal of Railway Science and Engineering, 21(1), pp. 183-193. DOI: 10.19713/j.cnki.43-1423/u.T20230282.

Zhang, Q. S., Dong, J. L., Leng, W. M., Zhang, C., Wen, C. P., Zhou, Z. H. (2024). Dynamic stress response in a novel prestressed subgrade under heavy-haul train loading: a numerical analysis. Construction and building materials, 412, pp. 134749. DOI: 10.1016/j.conbuildmat.2023.134749.